

VERIX: Towards Verified Explainability of Deep Neural Networks

Min Wu, Haoze Wu, Clark Barrett

Stanford University
 {minwu, haozewan, barrett}@cs.stanford.edu

Abstract

We present VERIX, a first step towards verified explainability of machine learning models in safety-critical applications. Specifically, our *sound* and *optimal* explanations can guarantee prediction invariance against bounded perturbations. We utilise constraint solving techniques together with feature sensitivity ranking to efficiently compute these explanations. We evaluate our approach on image recognition benchmarks and a real-world scenario of autonomous aircraft taxiing.

1 Introduction

Broad deployment of artificial intelligence (AI) systems in safety-critical domains, such as autonomous driving and aircraft landing, necessitates the development of approaches for trustworthy AI. One key ingredient for trustworthiness is *explainability*: the ability for an AI system to communicate the reasons for its behaviour in terms that humans can understand.

Previous work on explainable AI includes well-known model-agnostic explainers which produce explanations that remain valid for nearby inputs in feature space. In particular, LIME (Ribeiro, Singh, and Guestrin 2016) and SHAP (Lundberg and Lee 2017) learn simple, and thus interpretable, models locally around a given input. Building on this work, Anchors (Ribeiro, Singh, and Guestrin 2018) attempts to identify a subset of such input explanations that are sufficient to ensure the corresponding output value. However, such approaches are heuristic and do not provide any formal guarantees. They are thus inappropriate for use in high-risk scenarios. For instance, if a loan application model used by a bank has an explanation claiming that it depends only on a user’s “age”, “employment type” and “salary range”, yet in actuality applicants with the same such attributes but different “gender” or “ethnicity” receive dissimilar loan decisions, then the explanation is not only wrong, but may mask the actual bias in the model. Another drawback of model-agnostic approaches is that they depend on access to training data, which may not always be available (perhaps due to privacy concerns). And even if available, distribution shift can compromise the results.

Recent efforts towards *formal* explainable AI (Marques-Silva and Ignatiev 2022) aim to compute rigorously defined explanations that can guarantee *soundness*, in the sense that

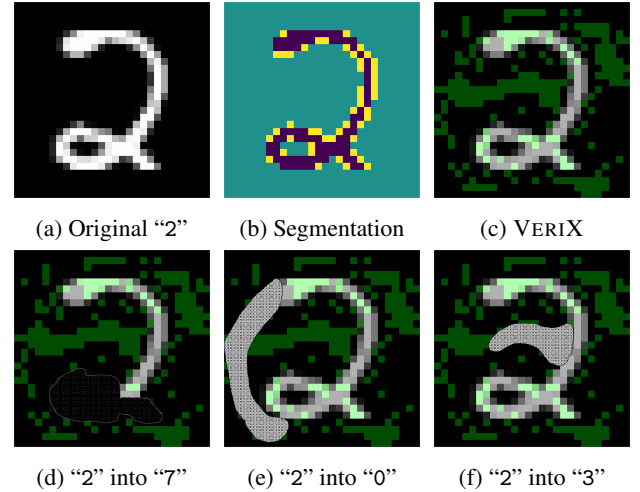


Figure 1: Intuition for our VERIX approach: (a) An MNIST handwritten “2” digit; (b) Segmentation of “2” into 3 partitions; (c) VERIX explanation (green pixels) of “2”; (d)(e)(f) Masking white pixels or whitening black pixels may turn “2” into “7”, “0”, or “3”.

fixing certain input features is sufficient to ensure the invariance of a model’s prediction (see Section 5 for a more detailed discussion). Unfortunately, these approaches are unable to tackle state-of-the-art deep neural networks and may extract unnecessarily complicated explanations, hindering the ability of humans to understand the model’s behaviour.

In this paper, we present VERIX (VERIFIED explainability) as a step towards computing sound and reliable explanations for deep neural networks. Our explanations guarantee prediction invariance against bounded perturbations imposed upon irrelevant input features. We provide intuition for our VERIX approach by analysing an example explanation for the MNIST digit “2” in Figure 1. The original digit is shown in Figure 1a. Anchors, mentioned above, relies on partitioning an image into a disjoint set of segments and then selecting the most prominent segment(s). Figure 1b shows “2” divided into 3 parts using k-means clustering (Lloyd 1982). Based on this segmentation, the purple and yellow parts would be chosen for the explanation, suggesting that

the model largely relies on these pixels to make its decision. This also matches our intuition, as a human would immediately identify these pixels as containing information and disregard the background. However, does this mean it is enough to focus on the salient features when explaining a classifier’s prediction? Not necessarily. VERIX’s explanation is highlighted in green in Figure 1c. It demonstrates that *whatever is prominent is important but what is absent in the background also matters*. We observe that VERIX not only marks those white pixels forming the silhouette of “2” but also includes some background pixels that might affect the prediction if changed. For instance, neglecting the bottom white pixels may lead to a misclassification as a “7”; meanwhile, the classifier also needs to check if the pixels along the left and in the middle are not white to make sure it is not “0” or “3”. While Figures 1d, 1e, and 1f are simply illustrative examples to provide intuition about why different parts of the explanation may be present, we remark that all the VERIX explanations are produced automatically and deterministically.

2 VERIX: Verified Explainability

Let \mathcal{N} be a neural network and \mathbf{x} be a d -dimensional input vector of features $\langle \chi^1, \dots, \chi^d \rangle$. We use $\Theta(\mathbf{x})$, or simply Θ , when the context is clear, to denote its set of feature indices $\{1, \dots, d\}$. We write \mathbf{x}^A where $A \subseteq \Theta(\mathbf{x})$ to denote only those features indexed by indices in A . We denote model prediction as $\mathcal{N}(\mathbf{x}) = c$, where c is a single quantity in regression or a label among others ($c \in C$) in classification. For the latter, we use $\mathcal{N}_c(\mathbf{x})$ to denote the confidence value (pre- or post- softmax) of classifying as c , i.e., $\mathcal{N}(\mathbf{x}) = \arg \max \mathcal{N}_c(\mathbf{x})$. Though we illustrate our VERIX framework using image classification networks, where \mathbf{x} is an image consisting of d pixels, it can also generalise to other machine learning domains such as natural language processing, where \mathbf{x} is a text of d words and each χ denotes a word embedding. Our motivation for focusing on images in this paper is that their explanations are self-illustrative and thus easier to understand.

2.1 Guaranteed Explanations

We define an *explanation* as a subset of the features in an input, representing those inputs responsible for a model’s prediction. Formally, an explanation is a set of features \mathbf{x}^A with $A \subseteq \Theta(\mathbf{x})$ that is sufficient to ensure that a model \mathcal{N} makes a specific prediction even if the remaining features \mathbf{x}^B (with $B = \Theta(\mathbf{x}) \setminus A$) are perturbed. We use ϵ to bound the perturbation on \mathbf{x}^B so as to be able to explore explanations of varying strength.

Definition 1 (Guaranteed Explanation). *Given a network \mathcal{N} , an input \mathbf{x} , a manipulation magnitude ϵ , and a discrepancy δ , a guaranteed explanation with respect to norm p is a set of input features \mathbf{x}^A such that if $B = \Theta(\mathbf{x}) \setminus A$, then*

$$\forall \mathbf{x}^{B'}. \left\| \mathbf{x}^B - \mathbf{x}^{B'} \right\|_p \leq \epsilon \Rightarrow |\mathcal{N}(\mathbf{x}) - \mathcal{N}(\mathbf{x}')| \leq \delta, \quad (1)$$

where $\mathbf{x}^{B'}$ is some perturbation on features \mathbf{x}^B , \mathbf{x}' is the input variant combining \mathbf{x}^A and $\mathbf{x}^{B'}$, and $p \in \{1, 2, \infty\}$ is Manhattan, Euclidean, or Chebyshev distance, respectively.

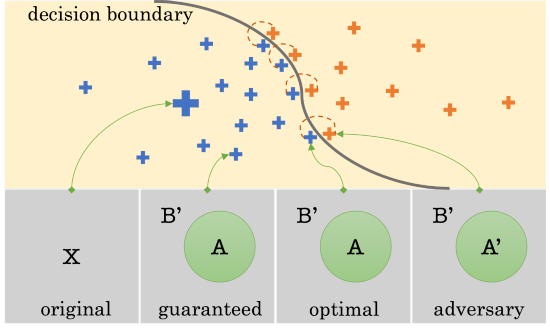


Figure 2: Graphical illustration of VERIX. The grey square at the left represents the features of an input \mathbf{x} , shown also as a big blue “+” in feature space. Variations of \mathbf{x} that do not change the explanation \mathbf{A} , shown as a green circle, are guaranteed to lie on the same side of the decision boundary as \mathbf{x} . On the other hand, if some feature in the green circle is changed (i.e., $\mathbf{A}' \neq \mathbf{A}$), then the result may be different.

The role of δ is to measure the prediction discrepancy. For classification models, we set δ to 0. For regression models, δ could be some pre-defined hyper-parameter quantifying allowable output change. We refer to \mathbf{x}^B as the *irrelevant* features. Intuitively, for classification models, a perturbation bounded by ϵ imposed upon the irrelevant features \mathbf{x}^B will *never* change the prediction. Figure 2 illustrates a guaranteed explanation, showing an original input \mathbf{x} and several variants. Those that do not perturb the explanation features \mathbf{A} are guaranteed to have the same prediction as \mathbf{x} .

2.2 Optimal Towards Model Decision Boundary

While there are infinitely many variants in the input space, we are particularly interested in those that lie along the decision boundary of a model. Figure 2 shows several pairs of variants (blue and orange “+”) connected red dotted lines. Each pair has the property that the blue variant produces the same result as the original input \mathbf{x} , whereas the orange variant, obtained by perturbing only one feature χ in the blue variant, produces a different result. Those key features are thus *indispensable* when explaining the decision-making process. With this insight, we define an *optimal* guaranteed explanation \mathbf{x}^A such that for each feature present in \mathbf{x}^A , a change can be made to produce a different result.

Definition 2 (Optimal Explanation). *Given a guaranteed explanation \mathbf{x}^A for a network \mathcal{N} , with irrelevant features \mathbf{x}^B , input \mathbf{x} , magnitude ϵ , and discrepancy δ , we say that \mathbf{x}^A is optimal if*

$$\forall \chi \in \mathbf{x}^A. \exists \mathbf{x}^{B'}, \chi'. \left\| (\mathbf{x}^B \oplus \chi) - (\mathbf{x}^{B'} \oplus \chi') \right\|_p \leq \epsilon \wedge |\mathcal{N}(\mathbf{x}) - \mathcal{N}(\mathbf{x}')| > \delta, \quad (2)$$

where $\mathbf{x}^{B'}$ and χ' denote some perturbations of \mathbf{x}^B and χ and \oplus denotes concatenation of two features.

Intuitively, each feature in the optimal explanation can be perturbed (together with the irrelevant features) to change

χ^1	χ^2	χ^3	χ^1	χ^2	χ^3	χ^1	χ^2	χ^3
χ^4	χ^5	χ^6	χ^4	χ^5	χ^6	χ^4	χ^5	χ^6
χ^7	χ^8	χ^9	χ^7	χ^8	χ^9	χ^7	χ^8	χ^9
χ^1	χ^2	χ^3	χ^1	χ^2	χ^3	χ^1	χ^2	χ^3
χ^4	χ^5	χ^6	χ^4	χ^5	χ^6	χ^4	χ^5	χ^6
χ^7	χ^8	χ^9	χ^7	χ^8	χ^9	χ^7	χ^8	χ^9
χ^1	χ^2	χ^3	χ^1	χ^2	χ^3	χ^1	χ^2	χ^3
χ^4	χ^5	χ^6	χ^4	χ^5	χ^6	χ^4	χ^5	χ^6
χ^7	χ^8	χ^9	χ^7	χ^8	χ^9	χ^7	χ^8	χ^9

Figure 3: Computing an optimal guaranteed explanation by constraint solving for a simple input $\mathbf{x} = \langle \chi^1, \dots, \chi^9 \rangle$. Grey denotes irrelevant features \mathbf{x}^B ; green is the optimal explanation \mathbf{x}^A .

the prediction. We mention two special cases: (1) if \mathbf{x} is ϵ -robust, then all features are irrelevant, i.e., $\mathbf{A} = \emptyset$, meaning there is no valid explanation as any ϵ -perturbation does not affect the prediction at all (in other words, a larger ϵ is required to get a meaningful explanation); (2) if perturbing any feature in input \mathbf{x} can change the prediction, then $\mathbf{A} = \Theta(\mathbf{x})$, meaning the entire input is an explanation.

We remark that our definition of optimal is *local* in that it is defined with respect to a specific set of features. This type of explanations is also referred to as abductive explanations (Ignatiev, Narodytska, and Marques-Silva 2019) or PI-explanations (Shih, Choi, and Darwiche 2018). An interesting problem would be to find a *globally optimal* explanation, that is, the one that is the smallest (i.e. fewest features) among all possible optimal explanations. A naive approach for computing such globally optimal explanations is extremely computationally difficult. In this paper, we propose an approximation that works well in practice and leave further improvements towards computing globally optimal explanations to future work.

3 Computing Guaranteed Explanations by Constraint Solving

The VERIX algorithm is shown as Algorithm 1. Before presenting it in detail, we first illustrate it via a simple example.

Example 1 (VERIX Computation). *Suppose \mathbf{x} is an input with 9 features $\langle \chi^1, \dots, \chi^9 \rangle$, and we have classification network \mathcal{N} , a perturbation magnitude ϵ , and are using $p = \infty$. The outer loop of the algorithm traverses of the input features. For simplicity, assume the order of the traversal is from χ^1 to χ^9 . Both the explanation index set \mathbf{A} and the irrelevant set \mathbf{B} are initialised to \emptyset . At each iteration, VERIX decides whether to add the index i to \mathbf{A} or \mathbf{B} . The evolution of the index sets is shown in Table 1. Concretely, when $i = 1$, VERIX formulates a pre-condition which specifies*

Algorithm 1: VERIX (VERIfied explainability)

Input: neural network \mathcal{N} and input $\mathbf{x} = \langle \chi^1, \dots, \chi^d \rangle$
Parameter: ϵ -perturbation, norm p , and discrepancy δ
Output: optimal explanation \mathbf{x}^A

```

1: function VERIX( $\mathcal{N}$ ,  $\mathbf{x}$ )
2:    $\mathbf{A}, \mathbf{B} \mapsto \emptyset, \emptyset$ 
3:    $c \mapsto \mathcal{N}(\mathbf{x})$ 
4:    $\hat{c} \mapsto \mathcal{N}(\hat{\mathbf{x}})$ 
5:    $\pi \mapsto \text{TRAVERSALORDER}(\mathbf{x})$ 
6:   for  $i$  in  $\pi$  do
7:      $\mathbf{B}' \mapsto \mathbf{B} \cup \{i\}$ 
8:      $\phi \mapsto (\|\hat{\mathbf{x}}^{\mathbf{B}'} - \mathbf{x}^{\mathbf{B}'}\|_p \leq \epsilon)$ 
9:      $\phi \mapsto \phi \wedge (\hat{\mathbf{x}}^{\Theta \setminus \mathbf{B}'} = \mathbf{x}^{\Theta \setminus \mathbf{B}'})$ 
10:    HOLD  $\mapsto \text{CHECK}(\mathcal{N}, \phi \Rightarrow |\hat{c} - c| \leq \delta)$ 
11:    if HOLD then  $\mathbf{B} \mapsto \mathbf{B}'$ 
12:    else  $\mathbf{A} \mapsto \mathbf{A} \cup \{i\}$ 
13:   return  $\mathbf{x}^A$ 

```

that χ^1 can be perturbed by ϵ while the other features remain unchanged. An automated reasoner is then invoked to check whether the pre-condition logically implies the post-condition (in this case, $\mathcal{N}(\mathbf{x}) = \mathcal{N}(\hat{\mathbf{x}})$, meaning the prediction is the same after perturbation). Suppose the reasoner returns **True**; then, no ϵ -perturbation on χ^1 can alter the prediction. Following Definition 1, we thus add χ^1 to the irrelevant features \mathbf{x}^B . Figure 3, top left, shows a visualisation of this. VERIX next moves on to χ^2 . This time the precondition allows ϵ -perturbations on both χ^1 and χ^2 while keeping the other features unchanged. The post-condition remains the same. Suppose the reasoner returns **True** again – we then add χ^2 to \mathbf{x}^B (Figure 3, top middle). Following similar steps, we add χ^3 to \mathbf{x}^B (Figure 3, top right). When it comes to χ^4 , we allow ϵ -perturbations for $\langle \chi^1, \chi^2, \chi^3, \chi^4 \rangle$ while the other features are fixed. Suppose this time the reasoner returns **False** – there exists a counterexample that violates $\mathcal{N}(\mathbf{x}) = \mathcal{N}(\hat{\mathbf{x}})$, i.e., the prediction can be different. Then, according to Definition 2, we add χ^4 to the optimal explanation \mathbf{x}^A (shown as green in Figure 3, middle left). The computation continues until all the input features are visited. Eventually, we have $\mathbf{x}^A = \langle \chi^4, \chi^5, \chi^8 \rangle$ (Figure 3, bottom right), which means that, if the features in the explanation are fixed, the model’s prediction is invariant to any ϵ -perturbation on the other features. Additionally, if any of the features in \mathbf{x}^A are added to the irrelevant set, the model can find a way to change the prediction..

3.1 Building Optimal Explanations Iteratively

We now formally describe our VERIX approach, which exploits an automated reasoning engine for neural network verification as a black-box sub-procedure. We assume the reasoner takes as inputs a network \mathcal{N} and a specification

$$\phi_{in}(\hat{\mathbf{x}}) \Rightarrow \phi_{out}(\hat{c}) \quad (3)$$

where $\hat{\mathbf{x}}$ are variables representing the network inputs and \hat{c} are expressions representing the network outputs. $\phi_{in}(\hat{\mathbf{x}})$

feature	A	B	B'	reasoner	irrelevant features \mathbf{x}^B	explanation \mathbf{x}^A
χ^1	\emptyset	\emptyset	$\mathbf{B} \cup \{1\}$	True	$\langle \chi^1 \rangle$	—
χ^2	\emptyset	$\{1\}$	$\mathbf{B} \cup \{2\}$	True	$\langle \chi^1, \chi^2 \rangle$	—
χ^3	\emptyset	$\{1, 2\}$	$\mathbf{B} \cup \{3\}$	True	$\langle \chi^1, \chi^2, \chi^3 \rangle$	—
χ^4	\emptyset	$\{1, 2, 3\}$	$\mathbf{B} \cup \{4\}$	False	$\langle \chi^1, \chi^2, \chi^3 \rangle$	$\langle \chi^4 \rangle$
χ^5	$\{4\}$	$\{1, 2, 3\}$	$\mathbf{B} \cup \{5\}$	False	$\langle \chi^1, \chi^2, \chi^3 \rangle$	$\langle \chi^4, \chi^5 \rangle$
χ^6	$\{4, 5\}$	$\{1, 2, 3\}$	$\mathbf{B} \cup \{6\}$	True	$\langle \chi^1, \chi^2, \chi^3, \chi^6 \rangle$	$\langle \chi^4, \chi^5 \rangle$
χ^7	$\{4, 5\}$	$\{1, 2, 3, 6\}$	$\mathbf{B} \cup \{7\}$	True	$\langle \chi^1, \chi^2, \chi^3, \chi^6, \chi^7 \rangle$	$\langle \chi^4, \chi^5 \rangle$
χ^8	$\{4, 5\}$	$\{1, 2, 3, 6, 7\}$	$\mathbf{B} \cup \{8\}$	False	$\langle \chi^1, \chi^2, \chi^3, \chi^6, \chi^7 \rangle$	$\langle \chi^4, \chi^5, \chi^8 \rangle$
χ^9	$\{4, 5, 8\}$	$\{1, 2, 3, 6, 7\}$	$\mathbf{B} \cup \{9\}$	True	$\langle \chi^1, \chi^2, \chi^3, \chi^6, \chi^7, \chi^9 \rangle$	$\langle \chi^4, \chi^5, \chi^8 \rangle$

Table 1: Evolving constraints and optimal explanation \mathbf{x}^A along reasoning result (True/False) when processing Example 1.

and $\phi_{out}(\hat{c})$ are formulas. We use $\hat{\chi}^i$ to denote the variable corresponding to the i^{th} feature. The reasoner checks whether a specification holds on a network.

As shown in Algorithm 1, the VERIX procedure takes as input a network \mathcal{N} and an input $\mathbf{x} = \langle \chi^1, \dots, \chi^d \rangle$. It outputs an optimal explanation \mathbf{x}^A with respect to perturbation magnitude ϵ , distance metric p , and discrepancy δ . The procedure maintains two sets, **A** and **B** throughout: **A** comprises feature indices forming the explanation, whereas **B** includes feature indices that can be excluded from the explanation. Recall that \mathbf{x}^B denotes the *irrelevant* features (i.e., perturbing \mathbf{x}^B while leaving \mathbf{x}^A unchanged never changes the prediction). To start with, these two sets are initialised as \emptyset (Line 2), and input \mathbf{x} is predicted as c , for which we remark that c may or may not be an *accurate* prediction according to the ground truth – VERIX generates an explanation regardless. Overall, the procedure examines every feature χ^i in \mathbf{x} according to TRAVERSALORDER (Line 5) to determine whether i can be added to **B** or must belong to **A**. The traversal order can significantly affect the size and shape of the explanation. We propose a heuristic for computing a traversal order that aims to produce small explanations in Section 3.2 (in Example 1, a sequential order is used for ease of explanation). For each i , we compute ϕ , a formula that encodes two conditions: (i) the current χ^i and \mathbf{x}^B are allowed to be perturbed by at most ϵ (Line 8); and (ii) the rest features are fixed (Line 9). The property that we check is that ϕ implies $|\hat{c} - c| \leq \delta$ (Line 10) denoting prediction invariance.

An automated reasoning sub-procedure CHECK is deployed to check whether on network \mathcal{N} the specification $\phi \Rightarrow |\hat{c} - c| \leq \delta$ holds (Line 10) – i.e., whether perturbing the current χ^i and irrelevant features while fixing the rest ensures a consistent prediction – it returns True if this is the case and False if not. In practice, this can be instantiated with an off-the-shelf neural network verification tool (Singh et al. 2019b; Müller et al. 2022; Katz et al. 2019; Wang et al. 2021; Henriksen and Lomuscio 2020). If CHECK returns True, i is added to the irrelevant set **B** (Line 11). Otherwise, i is added to the explanation index set **A** (Line 12), which conceptually indicates that χ^i contributes to the explanation of the prediction (since feature indices in **B** have already been proven to not affect prediction). In other words,

an ϵ -perturbation that includes the irrelevant features as well as the current χ^i can breach the decision boundary of \mathcal{N} . The procedure continues until all feature indices in \mathbf{x} are traversed and placed into one of the two disjoint sets **A** and **B**. At the end, \mathbf{x}^A is returned as the optimal explanation.

To ensure the procedure returns a guaranteed explanation, we require that CHECK is *sound*, i.e., the solver returns True only if the specification actually holds. For the guaranteed explanation to be optimal, CHECK also needs to be *complete*, i.e., the solver always returns True if the specification holds. We can incorporate various existing reasoners as the CHECK sub-routine. We note that an incomplete reasoner (the solver may return Unknown), does *not* undermine the soundness of our approach, though it does affect optimality (the produced explanations may be larger than necessary). Below we state these two properties of the VERIX procedure. Rigorous proofs are in Appendix A.

Lemma 1. *If CHECK is sound, at the end of each iteration in Algorithm 1, the irrelevant set of indices **B** satisfies*

$$(\|\hat{\chi}^{\mathbf{B}'} - \chi^{\mathbf{B}'}\|_p \leq \epsilon) \wedge (\hat{\chi}^{\Theta \setminus \mathbf{B}'} = \chi^{\Theta \setminus \mathbf{B}'}) \Rightarrow |\hat{c} - c| \leq \delta.$$

Intuitively, any ϵ -perturbation imposed upon all irrelevant features when fixing the others will always keep prediction consistent, i.e., those infinite number of input variants (small blue “+” in Figure 2) will always remain within the decision boundary. This can be proven by induction on the number of iterations. Soundness directly derives from Lemma 1.

Theorem 1 (Soundness). *If CHECK is sound, then the value \mathbf{x}^A returned by Algorithm 1 is a guaranteed explanation.*

Theorem 2 (Optimality). *If CHECK is sound and complete, then the guaranteed explanation \mathbf{x}^A returned by Algorithm 1 is optimal.*

Intuitively, optimality holds because if it is not possible for an ϵ -perturbation on some feature χ^i in explanation \mathbf{x}^A to change the prediction, then it will be added to the irrelevant features \mathbf{x}^B when feature χ^i is considered during the execution of Algorithm 1.

Proposition 1 (Complexity). *Given a d -dimensional input \mathbf{x} and a network \mathcal{N} , the complexity of computing an optimal explanation is $O(d \cdot P(\mathcal{N}))$, where $P(\mathcal{N})$ is the cost of checking a specification (as in Equation 3) over \mathcal{N} .*

Note that an optimal explanation can be achieved from one traversal of input features. If \mathcal{N} is piecewise-linear, checking a specification over \mathcal{N} is NP-complete (Katz et al. 2017).

3.2 Feature-Level Sensitivity Traversal

Example 1 used a straightforward left-to-right and top-to-bottom traversal order. Here we introduce a heuristic based on *feature-level sensitivity*, inspired by the occlusion method (Zeiler and Fergus 2014).

Definition 3 (Sensitivity). *Given an input $\mathbf{x} = \langle x^1, \dots, x^d \rangle$ and a network \mathcal{N} , the feature-level sensitivity (in classification for a label c or in regression for a single quantity) for a feature x^i with respect to a transformation \mathcal{T} is*

$$\text{sensitivity}(x^i) = \mathcal{N}_{(c)}(\mathbf{x}) - \mathcal{N}_{(c)}(\mathbf{x}'), \quad (4)$$

where \mathbf{x}' is \mathbf{x} with x^i replaced by $\mathcal{T}(x^i)$.

Typical transformations include deletion ($\mathcal{T}(x) = 0$) and reversal ($\mathcal{T}(x) = \bar{x} - x$, where \bar{x} is the maximum value for feature x). Intuitively, we measure how sensitive (in terms of an increase or decrease) a model’s confidence is to each individual feature. Given sensitivity values with respect to some transformation, we rank the feature indices into a traversal order from least sensitive to most sensitive.

4 Experimental Results

We have implemented the VERIX algorithm in Python¹, using the Marabou (Katz et al. 2019) neural network verification tool to implement CHECK (Algorithm 1, Line 10). Marabou’s Python API supports specification encoding and incremental solving, making it a good fit. We trained fully-connected and convolutional networks on the MNIST (Le-Cun, Cortes, and Burges 2010), GTSRB (Stallkamp et al. 2012), and TaxiNet (Julian, Lee, and Kochenderfer 2020) datasets for classification and regression tasks. Model specifications are in Appendix B. Experiments were performed on a cluster equipped with Intel Xeon E5-2637 v4 CPUs running Ubuntu 16.04. We set a time limit of 300 seconds for each CHECK call.

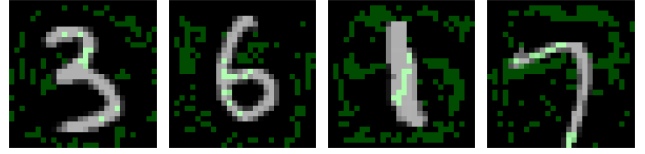
4.1 Example Explanations

Figure 4 shows examples of VERIX explanations for GTSRB and MNIST images. Aligning with our intuition, VERIX can distinguish the traffic signs (no matter a circle, a triangle, or a square in Figure 6a) from their surroundings well; the explanations focus on the actual contents within the signs, e.g., the right arrow denoting “keep right” and the number 50 as in “50 mph”. Interestingly, for traffic signs consisting of irregular dark shapes on a white background such as “road work” and “no passing”, VERIX discovers that the white background contains the essential features. We notice that MNIST explanations are in general more scattered around the background because the network relies on the non-existence of white pixels to recognise certain digits (e.g., the classifier requires an empty top region to predict a “7” instead of a “9” as shown in Figure 4b last column),

¹The VERIX code is available at <https://github.com/NeuralNetworkVerification/VeriX>.

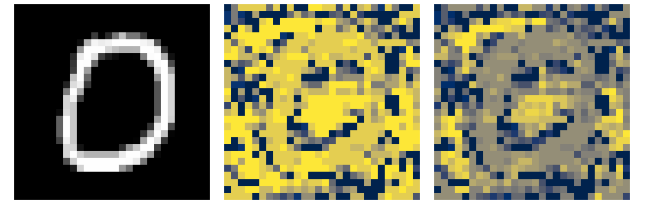


(a) “keep right”, “50 mph”, “road work”, “no passing”

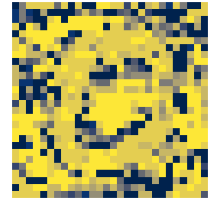


(b) “3”, “6”, “1”, and “7”

Figure 4: Optimal explanations (green) from VERIX on GTSRB (top) and MNIST (bottom) images.



(a) MNIST “0”



(b) $\epsilon : 100\% \rightarrow 10\%$



(c) $\epsilon : 100\% \rightarrow 5\%$

Figure 5: Visualisation of the expansion of the irrelevant pixels when perturbation magnitude ϵ decreases from 100% to 10% and further to 5% (from deep blue to light yellow). Each brighter colour denotes the pixels added when moving to the next smaller ϵ , e.g., 100%, 90%, 80% and so on.

whereas GTSRB explanations can safely disregard the surrounding pixels outside the traffic signs.

4.2 Effect of Varying ϵ -Perturbations

A key parameter of VERIX is the perturbation bound ϵ . When ϵ is varied, the irrelevant features change accordingly. Figure 5 visualises this, showing how the irrelevant features change ϵ is varied from 100% to 10% and further to 5%. As ϵ decreases, more pixels become irrelevant. Intuitively, the VERIX explanation helps reveal how the network classifies this image as 0. The deep blue pixels are those that are irrelevant with $\epsilon = 100\%$. Light blue pixels are more sensitive, allowing only perturbations of only 10%. The light yellow pixels represent 5%, and bright yellow are pixels that cannot even be perturbed 5% without changing the prediction. The resulting pattern is roughly consistent with our intuition, as the shape of the 0 can be seen embedded in the explanation.

We remark that choosing an appropriate perturbation magnitude ϵ is non-trivial because if ϵ is too loose, explanations may be too conservative, allowing very few pixels to change. On the other hand, if ϵ is too small, nearly the whole set of pixels could become irrelevant. For instance, in Figure 5, if we set ϵ to 1% then all pixels become irrelevant – the classifier’s prediction is robust to perturbations of 1%. The “colour map” we propose makes it possible to visualise

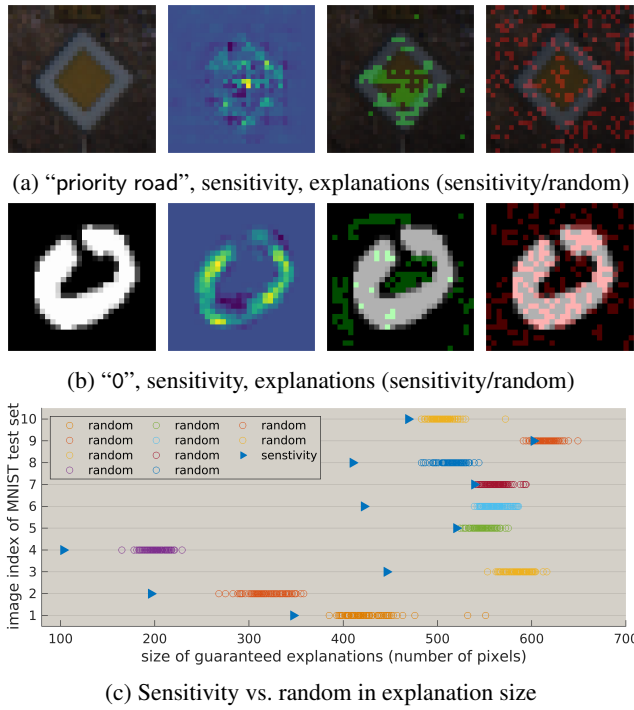


Figure 6: Comparing VERIX explanations, when using *sensitivity* (green) and random (red) traversals, on GTSRB and MNIST. (c) Each blue triangle denotes 1 deterministic explanation from sensitivity ranking, and each bunch of circles represents 100 random traversals.

not only the explanation but also how it varies with ϵ . The user then has the freedom to pick a specific ϵ depending on their application.

4.3 Sensitivity vs. Random Traversal

To show the advantage of the *sensitivity* traversal (described in Section 3.2), Figure 6 compares VERIX explanations using sensitivity-based and random traversal orders. The first column shows the original image; the second a heatmap of the sensitivity (with $\mathcal{T}(\chi) = 0$); and the third and fourth columns show explanations using the sensitivity and random traversal orders, respectively. Sensitivity, as shown in the heatmaps, prioritises pixels that have less influence on the network’s prediction. In contrast, a random ranking is simply a shuffling of all the pixels. We observe that the sensitivity traversal generates smaller and more sensible explanations. In Figure 6, we compare explanation sizes for the first 10 images (to avoid potential selection bias) of the MNIST test set. For each image, we show 100 random traversal explanations compared to the sensitivity traversal explanation. We notice that the latter is almost always smaller, often significantly so, suggesting that sensitivity-based traversals are a reasonable heuristic for attempting to approach globally optimal explanations.

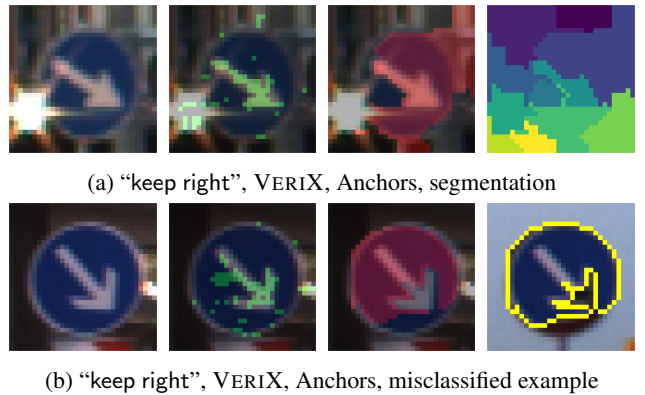


Figure 7: Comparing VERIX (green) to Anchors (red) on two versions of a “keep right” traffic sign, one with strong light in the background and one without.

	MNIST		GTSRB	
	size	time	size	time
VERIX (sensitivity)	180.6	174.77	357.0	853.91
VERIX (random)	294.2	157.47	383.5	814.18
Anchors	494.9	13.46	557.7	26.15

Table 2: VERIX vs. Anchors regarding average explanation size (number of pixels) and generation time (seconds). In VERIX, ϵ is set to 5% for MNIST and 0.5% for GTSRB.

4.4 VERIX vs. Anchors

We compare our VERIX approach with Anchors (Ribeiro, Singh, and Guestrin 2018). Figure 7 shows both approaches applied to two different versions of a “keep right” traffic sign. Anchors performs image segmentation and selects a set of the segments as the explanation, making its explanations heavily dependent on the quality of the segmentation. For instance, distractions such as strong light in the background may compromise the segments (Figure 7a, last column) thus resulting in less-than-ideal explanations, e.g., the top right region of the anchor (red) is outside the actual traffic sign. As described above, VERIX utilises the model to compute the sensitivity traversal, often leading to more reasonable explanations. Anchors is also not designed to provide *formal* guarantees. In fact, replacing the background of an anchor explanation can change the classification. For example, the last column of Figure 7b is classified as “yield” with confidence 99.92%.

Two key metrics for evaluating the quality of an explanation are the *size* and the *generation time*. Table 2 shows that overall, VERIX produces much smaller explanations than Anchors. On the other hand, it takes much longer to perform the computation necessary to ensure formal guarantees. The two techniques thus provide a trade-off between time and explanation quality. Table 2 also shows that sensitivity traversals produce significantly smaller sizes with only a modest overhead in time.

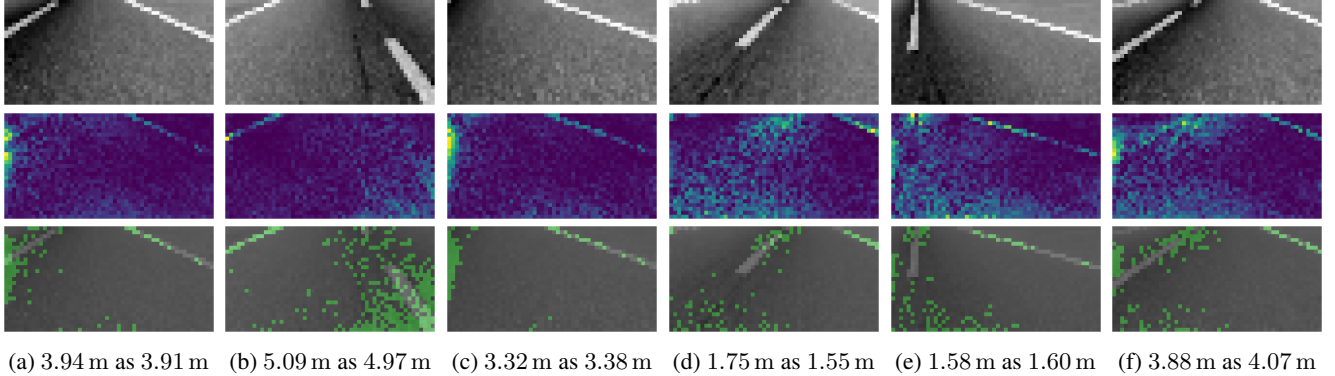


Figure 8: VERIX applied to the TaxiNet dataset – each column includes a sampled camera view (top), its sensitivity (middle), and the cross-track estimate (in meters).

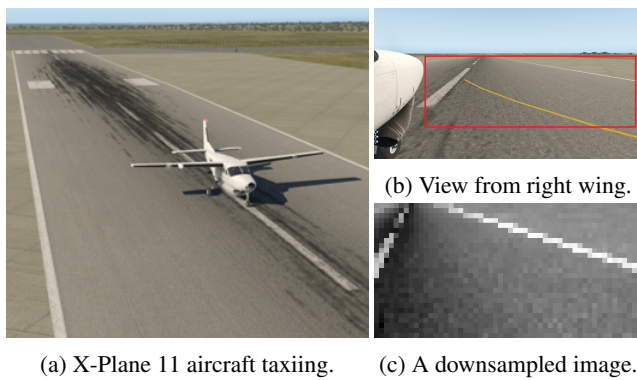


Figure 9: An autonomous aircraft taxiing scenario (Julian, Lee, and Kochenderfer 2020). Pictures taken from the camera on the right wing of the aircraft are cropped (red box) and downsampled to obtain the TaxiNet dataset.

4.5 Vision-Based Autonomous Aircraft Taxiing

We applied VERIX to the real-world safety-critical aircraft taxiing scenario (Julian, Lee, and Kochenderfer 2020) shown in Figure 9. The vision-based autonomous taxiing system needs to make sure the aircraft stays on the taxiway utilising only pictures taken from the camera on the right wing. The task is to evaluate the cross-track position of the aircraft so that a controller can adjust its position accordingly. To achieve this, a regression model is used that takes a picture as input and produces an estimate of the current position. A preprocessing step crops out the sky and aircraft nose, keeping the crucial taxiway region (in the red box). This is then downsampled into a grey-scale image of size 27×54 pixels. We label each image with its corresponding lateral distance to the runway centerline as well as the taxiway heading angle. We train a fully connected feed-forward network on this dataset, referred to as TaxiNet (Julian, Lee, and Kochenderfer 2020), to predict the aircraft’s cross-track distance.

Figure 8 shows VERIX applied to TaxiNet, including a variety of taxiway images with different heading angles and

number of lanes. For each taxiway, we show its VERIX explanation accompanied by a sensitivity heatmap and the cross-track estimate. We observe that the model is capable of detecting the more remote line – its contour is clearly marked in green. Meanwhile, the model is mainly focused on the centerline (especially in Figures 8b, 8d, 8e, and 8f), which makes sense as it needs to measure how far the aircraft has deviated from the center. Interestingly, while we intuitively might assume that the model would focus on the white lanes and discard the rest, VERIX shows that the bottom middle region is also crucial to the explanation (e.g., as shown in Figures 8a and 8c). This is because the model must take into account the presence and absence of the centerline. This is in fact in consistent with our observations about the black background in MNIST images (Figure 1). We used $\epsilon = 5\%$ for these explanations, which suggests that for modest perturbations (e.g., brightness change due to different weather conditions) the predicted cross-track estimate will remain within an acceptable discrepancy, and taxiing will not be compromised.

4.6 Runtime Performance

We analyse the empirical time *complexity* of our VERIX approach in Table 3. The model structures are described in Appendix B.4. Typically, the individual pixel checks (CHECK) return a definitive answer (True or False) within a second on dense models and in a few seconds on convolutional networks. For image benchmarks such as MNIST and GTSRB, larger inputs or more complicated models result in longer (pixel- and image-level) execution times for generating explanations. As for TaxiNet as a regression task, while its pixel-level check takes longer than that of MNIST, it is actually faster in total time on dense models because TaxiNet does not need to check against other labels.

The *scalability* of VERIX can be improved if we perform incomplete verification, for which we re-emphasise that the soundness of the resulting explanations is not undermined. To illustrate, we deploy the incomplete CROWN (Zhang et al. 2018) analysis (implemented in Marabou) to perform the CHECK sub-procedure. Table 4 reports the runtime performance of VERIX when using incomplete verification on

	Dense		Dense (large)		CNN	
	CHECK	VERIX	CHECK	VERIX	CHECK	VERIX
MNIST (28 × 28)	0.013	160.59	0.055	615.85	0.484	4956.91
TaxiNet (27 × 54)	0.020	114.69	0.085	386.62	2.609	8814.85
GTSRB (32 × 32 × 3)	0.091	675.04	0.257	1829.91	1.574	12935.27

Table 3: Average execution time (seconds) of CHECK and VERIX for *complete* verification. In particular, ϵ is set to 3% across MNIST, TaxiNet, and GTSRB datasets for sensible comparison.

	# ReLU	# MaxPool	CHECK	VERIX
MNIST-sota	50960	5632	2.31	1841.25
GTSRB-sota	106416	5632	8.54	8770.15

Table 4: Average execution time (seconds) of CHECK and VERIX for *incomplete* verification. ϵ is 3% for both MNIST and GTSRB.

state-of-the-art network architectures with hundreds of thousands of neurons. See models in Appendix B, Tables 6 and 8. In general, the scalability of VERIX will grow with that of verification tools, which has improved significantly in the past several years as demonstrated by the results from the Verification of Neural Networks Competitions (VNN-COMP) (Bak et al. 2022).

5 Related Work

5.1 Formal Explanations

Existing work on formal explanations has significant limitations (Marques-Silva and Ignatiev 2022). First, in terms of *scalability*, they can only handle simple machine learning models such as naive Bayes classifiers (Marques-Silva et al. 2020), random forests (Izza and Marques-Silva 2021; Boumazouza et al. 2021), decision trees (Izza, Ignatiev, and Marques-Silva 2022), and boosted trees (Ignatiev 2020; Ignatiev et al. 2022). In particular, (Ignatiev, Narodytska, and Marques-Silva 2019) addresses networks with very simple structure (e.g., one hidden layer of 15 or 20 neurons) and reports only preliminary results. In contrast, VERIX works with state-of-the-art deep neural networks applicable to real-world safety-critical scenarios. Second, the *size* of explanations in existing work can be unnecessarily conservative. As a workaround, approximate explanations (Waeldchen et al. 2021; Wang, Khosravi, and Van den Broeck 2021) are proposed as a generalisation to provide probabilistic (thus compromised) guarantees of prediction invariance. VERIX, by utilising feature-level sensitivity ranking, produces reasonably-sized and sensible explanations (see our advantage over random traversal in Section 4.3) with rigorous guarantees. Third, current formal explanations allow *any possible input* in feature space, which is not necessary or even realistic. For instance, a lane perception model deployed in self-driving cars should be able to correctly recognise traffic signs all day and night, with brightness changes in a practical range, e.g., the road signs will not turn com-

pletely white (RGB values (255, 255, 255)). VERIX’s perturbation parameter ϵ allows us the flexibility to imitate physically plausible distortions.

5.2 Verification of Neural Networks

Researchers have investigated how automated reasoning can aid verification of neural networks with respect to formally specified properties (Liu et al. 2021; Huang et al. 2020), by utilising reasoners based on abstraction (Zhang et al. 2018; Singh et al. 2018, 2019a,b; Gehr et al. 2018; Tran et al. 2020; Müller et al. 2022; Wang et al. 2018a,b; Anderson et al. 2019; Zelazny et al. 2022; Wu et al. 2022a, 2023) and search (Ehlers 2017; Katz et al. 2017, 2019; Huang et al. 2017; Wang et al. 2021; Tjeng, Xiao, and Tedrake 2019; Henriksen and Lomuscio 2020; Bunel et al. 2020; De Palma et al. 2021; Ruan et al. 2019; Wu et al. 2020b; Wu and Kwiatkowska 2020; Botoeva et al. 2020; Khedr, Ferlez, and Shoukry 2021; Ferrari et al. 2022; Wu et al. 2020a, 2022b). Those approaches mainly focus on verifying whether a network satisfies a certain pre-defined property (e.g., robustness), i.e., either prove the property holds or disprove it with a counterexample. However, this does not shed light on *why* a network makes a specific prediction. We take a step further, repurposing those verification engines as sub-routines to inspect the decision-making process of a model, thereby explaining its behaviour (through the presence or absence of certain input features). The hope is that these explanations can help humans better interpret machine learning models and thus facilitate appropriate deployment.

6 Conclusions and Future Work

We have presented the VERIX approach for computing *sound* and *optimal* explanations for state-of-the-art deep neural networks, facilitating explainable and trustworthy AI in safety-critical domains. A possible future direction is generalising to other crucial network properties such as *fairness*. Recall the loan application model in Section 1; our approach can discover potential bias (if it exists) by including those “gender” and “ethnicity” attributes in the produced explanations; then a human decision-maker can better interpret the loan prediction outcomes to promote a fair and unbiased model.

References

Anderson, G.; Pailoor, S.; Dillig, I.; and Chaudhuri, S. 2019. Optimization and abstraction: a synergistic approach for analyzing neural network robustness. In *Proceedings of the 40th ACM SIGPLAN Conference on Programming Language Design and Implementation*, 731–744.

Bak, S.; Liu, C.; Johnson, T. T.; Brix, C.; and Müller, M. 2022. The 3rd International Verification of Neural Networks Competition (VNN-COMP). <https://sites.google.com/view/vnn2022>.

Botoeva, E.; Kouvaros, P.; Kronqvist, J.; Lomuscio, A.; and Misener, R. 2020. Efficient verification of relu-based neural networks via dependency analysis. In *Proceedings of the AAAI Conference on Artificial Intelligence*, volume 34, 3291–3299.

Boumazouza, R.; Cheikh-Alili, F.; Mazure, B.; and Tabia, K. 2021. ASTERYX: A model-Agnostic SaT-basEd appRoach for sYmbolic and score-based eXplanations. In *Proceedings of the 30th ACM International Conference on Information & Knowledge Management*, 120–129.

Bunel, R.; Turkaslan, I.; Torr, P. H.; Kumar, M. P.; Lu, J.; and Kohli, P. 2020. Branch and Bound for Piecewise Linear Neural Network Verification. *Journal of Machine Learning Research*, 21: 1–39.

De Palma, A.; Behl, H. S.; Bunel, R.; Torr, P.; and Kumar, M. P. 2021. Scaling the Convex Barrier with Active Sets. In *International Conference on Learning Representations*.

Ehlers, R. 2017. Formal verification of piece-wise linear feed-forward neural networks. In *International Symposium on Automated Technology for Verification and Analysis*, 269–286. Springer.

Ferrari, C.; Mueller, M. N.; Jovanović, N.; and Vechev, M. 2022. Complete Verification via Multi-Neuron Relaxation Guided Branch-and-Bound. In *International Conference on Learning Representations*.

Gehr, T.; Mirman, M.; Drachsler-Cohen, D.; Tsankov, P.; Chaudhuri, S.; and Vechev, M. 2018. AI2: Safety and robustness certification of neural networks with abstract interpretation. In *2018 IEEE symposium on security and privacy (SP)*, 3–18. IEEE.

Henriksen, P.; and Lomuscio, A. 2020. Efficient neural network verification via adaptive refinement and adversarial search. In *ECAI 2020*, 2513–2520. IOS Press.

Huang, X.; Kroening, D.; Ruan, W.; Sharp, J.; Sun, Y.; Thamo, E.; Wu, M.; and Yi, X. 2020. A survey of safety and trustworthiness of deep neural networks: Verification, testing, adversarial attack and defence, and interpretability. *Computer Science Review*, 37: 100270.

Huang, X.; Kwiatkowska, M.; Wang, S.; and Wu, M. 2017. Safety verification of deep neural networks. In *International conference on computer aided verification*, 3–29. Springer.

Ignatiev, A. 2020. Towards trustable explainable AI. In *Proceedings of the Twenty-Ninth International Conference on International Joint Conferences on Artificial Intelligence*, 5154–5158.

Ignatiev, A.; Izza, Y.; Stuckey, P. J.; and Marques-Silva, J. 2022. Using MaxSAT for efficient explanations of tree ensembles. In *Proceedings of the AAAI Conference on Artificial Intelligence*, volume 36, 3776–3785.

Ignatiev, A.; Narodytska, N.; and Marques-Silva, J. 2019. Abduction-based explanations for machine learning models. In *Proceedings of the AAAI Conference on Artificial Intelligence*, volume 33, 1511–1519.

Izza, Y.; Ignatiev, A.; and Marques-Silva, J. 2022. On Tackling Explanation Redundancy in Decision Trees. *J. Artif. Intell. Res.*, 75: 261–321.

Izza, Y.; and Marques-Silva, J. 2021. On Explaining Random Forests with SAT. In Zhou, Z.-H., ed., *Proceedings of the Thirtieth International Joint Conference on Artificial Intelligence, IJCAI-21*, 2584–2591. International Joint Conferences on Artificial Intelligence Organization. Main Track.

Julian, K. D.; Lee, R.; and Kochenderfer, M. J. 2020. Validation of image-based neural network controllers through adaptive stress testing. In *2020 IEEE 23rd international conference on intelligent transportation systems (ITSC)*, 1–7. IEEE.

Katz, G.; Barrett, C.; Dill, D. L.; Julian, K.; and Kochenderfer, M. J. 2017. Reluplex: An efficient SMT solver for verifying deep neural networks. In *International Conference on Computer Aided Verification*, 97–117. Springer.

Katz, G.; Huang, D. A.; Ibeling, D.; Julian, K.; Lazarus, C.; Lim, R.; Shah, P.; Thakoor, S.; Wu, H.; Zeljić, A.; et al. 2019. The marabou framework for verification and analysis of deep neural networks. In *International Conference on Computer Aided Verification*, 443–452.

Khedr, H.; Ferlez, J.; and Shoukry, Y. 2021. Peregrinn: Penalized-relaxation greedy neural network verifier. In *International Conference on Computer Aided Verification*, 287–300. Springer.

LeCun, Y.; Cortes, C.; and Burges, C. 2010. MNIST handwritten digit database. *ATT Labs [Online]. Available: <http://yann.lecun.com/exdb/mnist>*, 2.

Liu, C.; Arnon, T.; Lazarus, C.; Strong, C.; Barrett, C.; Kochenderfer, M. J.; et al. 2021. Algorithms for verifying deep neural networks. *Foundations and Trends® in Optimization*, 4(3-4): 244–404.

Lloyd, S. 1982. Least squares quantization in PCM. *IEEE transactions on information theory*, 28(2): 129–137.

Lundberg, S. M.; and Lee, S.-I. 2017. A unified approach to interpreting model predictions. In *Proceedings of the 31st International Conference on Neural Information Processing Systems*, 4768–4777.

Marques-Silva, J.; Gerspacher, T.; Cooper, M. C.; Ignatiev, A.; and Narodytska, N. 2020. Explaining naive bayes and other linear classifiers with polynomial time and delay. In *Proceedings of the 34th International Conference on Neural Information Processing Systems*, 20590–20600.

Marques-Silva, J.; and Ignatiev, A. 2022. Delivering Trustworthy AI through formal XAI. In *Proceedings of the AAAI Conference on Artificial Intelligence*, 3806–3814.

Müller, M. N.; Makarchuk, G.; Singh, G.; Püschel, M.; and Vechev, M. 2022. PRIMA: general and precise neural network certification via scalable convex hull approximations. *Proceedings of the ACM on Programming Languages*, 6(POPL): 1–33.

Ribeiro, M. T.; Singh, S.; and Guestrin, C. 2016. “Why should i trust you?” Explaining the predictions of any classifier. In *Proceedings of the 22nd ACM SIGKDD international conference on knowledge discovery and data mining*, 1135–1144.

Ribeiro, M. T.; Singh, S.; and Guestrin, C. 2018. Anchors: high-precision model-agnostic explanations. In *Proceedings of the Thirty-Second AAAI Conference on Artificial Intelligence and Thirtieth Innovative Applications of Artificial Intelligence Conference and Eighth AAAI Symposium on Educational Advances in Artificial Intelligence*, 1527–1535.

Ruan, W.; Wu, M.; Sun, Y.; Huang, X.; Kroening, D.; and Kwiatkowska, M. 2019. Global Robustness Evaluation of Deep Neural Networks with Provable Guarantees for the Hamming Distance. In *Proceedings of the Twenty-Eighth International Joint Conference on Artificial Intelligence*, IJCAI-19, 5944–5952.

Shih, A.; Choi, A.; and Darwiche, A. 2018. A symbolic approach to explaining Bayesian network classifiers. In *Proceedings of the 27th International Joint Conference on Artificial Intelligence*, 5103–5111.

Singh, G.; Ganvir, R.; Püschel, M.; and Vechev, M. 2019a. Beyond the single neuron convex barrier for neural network certification. In *Proceedings of the 33rd International Conference on Neural Information Processing Systems*, 15098–15109.

Singh, G.; Gehr, T.; Mirman, M.; Püschel, M.; and Vechev, M. 2018. Fast and effective robustness certification. In *Proceedings of the 32nd International Conference on Neural Information Processing Systems*, 10825–10836.

Singh, G.; Gehr, T.; Püschel, M.; and Vechev, M. 2019b. An abstract domain for certifying neural networks. *Proceedings of the ACM on Programming Languages*, 3(POPL): 1–30.

Stallkamp, J.; Schlipsing, M.; Salmen, J.; and Igel, C. 2012. Man vs. computer: Benchmarking machine learning algorithms for traffic sign recognition. *Neural networks*, 32: 323–332.

Tjeng, V.; Xiao, K. Y.; and Tedrake, R. 2019. Evaluating Robustness of Neural Networks with Mixed Integer Programming. In *International Conference on Learning Representations*.

Tran, H.-D.; Bak, S.; Xiang, W.; and Johnson, T. T. 2020. Verification of deep convolutional neural networks using im- agestars. In *International Conference on Computer Aided Verification*, 18–42. Springer.

Waeldchen, S.; Macdonald, J.; Hauch, S.; and Kutyniok, G. 2021. The computational complexity of understanding binary classifier decisions. *Journal of Artificial Intelligence Research*, 70: 351–387.

Wang, E.; Khosravi, P.; and Van den Broeck, G. 2021. Probabilistic Sufficient Explanations. In Zhou, Z.-H., ed., *Proceedings of the Thirtieth International Joint Conference on Artificial Intelligence*, IJCAI-21, 3082–3088. International Joint Conferences on Artificial Intelligence Organization. Main Track.

Wang, S.; Pei, K.; Whitehouse, J.; Yang, J.; and Jana, S. 2018a. Efficient formal safety analysis of neural networks. In *Proceedings of the 32nd International Conference on Neural Information Processing Systems*, 6369–6379.

Wang, S.; Pei, K.; Whitehouse, J.; Yang, J.; and Jana, S. 2018b. Formal security analysis of neural networks using symbolic intervals. In *Proceedings of the 27th USENIX Conference on Security Symposium*, 1599–1614.

Wang, S.; Zhang, H.; Xu, K.; Lin, X.; Jana, S.; Hsieh, C.-J.; and Kolter, Z. 2021. Beta-CROWN: Efficient Bound Propagation with Per-neuron Split Constraints for Neural Network Robustness Verification. In *Proceedings of the 35th Conference on Neural Information Processing Systems (NeurIPS)*, volume 34, 29909–29921.

Wu, H.; Barrett, C.; Sharif, M.; Narodytska, N.; and Singh, G. 2022a. Scalable Verification of GNN-Based Job Schedulers. *Proc. ACM Program. Lang.*, 6(OOPSLA2).

Wu, H.; Ozdemir, A.; Zeljić, A.; Julian, K.; Irfan, A.; Gopinath, D.; Fouladi, S.; Katz, G.; Pasareanu, C.; and Barrett, C. 2020a. Parallelization techniques for verifying neural networks. In *2020 Formal Methods in Computer Aided Design (FMCAD)*, 128–137. IEEE.

Wu, H.; Tagomori, T.; Robey, A.; Yang, F.; Matni, N.; Pappas, G.; Hassani, H.; Pasareanu, C.; and Barrett, C. 2023. Toward Certified Robustness Against Real-World Distribution Shifts. In *IEEE Conference on Secure and Trustworthy Machine Learning*.

Wu, H.; Zeljić, A.; Katz, G.; and Barrett, C. 2022b. Efficient Neural Network Analysis with Sum-of-Infeasibilities. In *International Conference on Tools and Algorithms for the Construction and Analysis of Systems*, 143–163. Springer.

Wu, M.; and Kwiatkowska, M. 2020. Robustness guarantees for deep neural networks on videos. In *Proceedings of the IEEE/CVF Conference on Computer Vision and Pattern Recognition*, 311–320.

Wu, M.; Wicker, M.; Ruan, W.; Huang, X.; and Kwiatkowska, M. 2020b. A game-based approximate verification of deep neural networks with provable guarantees. *Theoretical Computer Science*, 807: 298–329.

Zeiler, M. D.; and Fergus, R. 2014. Visualizing and understanding convolutional networks. In *European conference on computer vision*, 818–833. Springer.

Zelazny, T.; Wu, H.; Barrett, C.; and Katz, G. 2022. On Optimizing Back-Substitution Methods for Neural Network Verification. In *Formal Methods in Computer Aided Design (FMCAD)*, 17–26. IEEE.

Zhang, H.; Weng, T.-W.; Chen, P.-Y.; Hsieh, C.-J.; and Daniel, L. 2018. Efficient neural network robustness certification with general activation functions. In *Proceedings of the 32nd International Conference on Neural Information Processing Systems*, 4944–4953.

A Proofs for Theorems

We present rigorous proofs for Lemma 1, Theorems 1 and 2 in Section 3.1, justifying the *soundness* and *optimality* of our VERIX approach. For better readability, we repeat each lemma and theorem before their corresponding proofs.

A.1 Proof for Lemma 1

Lemma 1. *If CHECK is sound, at the end of each iteration in Algorithm 1, the irrelevant set of indices \mathbf{B} satisfies*

$$(\|\hat{\chi}^{\mathbf{B}'} - \chi^{\mathbf{B}'}\|_p \leq \epsilon) \wedge (\hat{\chi}^{\Theta \setminus \mathbf{B}'} = \chi^{\Theta \setminus \mathbf{B}'}) \Rightarrow |\hat{c} - c| \leq \delta.$$

Proof. Recall that the sub-procedure CHECK is sound means the deployed automated reasoner returns True only if the specification actually holds. That is, from Line 10 we have

$$\phi \Rightarrow |\hat{c} - c| \leq \delta$$

holds on network \mathcal{N} . Simultaneously, from Lines 8 and 9 we know that, to check the current feature χ^i of the traversing order π , the pre-condition ϕ contains

$$\phi \mapsto (\|\hat{\chi}^{\mathbf{B}'} - \chi^{\mathbf{B}'}\|_p \leq \epsilon) \wedge (\hat{\chi}^{\Theta \setminus \mathbf{B}'} = \chi^{\Theta \setminus \mathbf{B}'}).$$

Specifically, we prove this through induction on the number of iteration i . When i is 0, pre-condition ϕ is initialised as \top and the specification holds trivially. In the inductive case, suppose CHECK returns False, then the set \mathbf{B} is unchanged as in Line 12. Otherwise, if CHECK returns True, which makes HOLD become True, then the current feature index i is added into the irrelevant set of feature indices \mathbf{B} as in Line 11, with such satisfying specification

$$(\|\hat{\chi}^{\mathbf{B}'} - \chi^{\mathbf{B}'}\|_p \leq \epsilon) \wedge (\hat{\chi}^{\Theta \setminus \mathbf{B}'} = \chi^{\Theta \setminus \mathbf{B}'}) \Rightarrow |\hat{c} - c| \leq \delta.$$

As the iteration proceeds, each time CHECK returns True, the irrelevant set \mathbf{B} is augmented with the current feature index i , and the specification always holds as it is explicitly checked by the CHECK reasoner. \square

A.2 Proof for Theorem 1

Theorem 1 (Soundness). *If CHECK is sound, Algorithm 1 returns a guaranteed explanation $\mathbf{x}^{\mathbf{A}}$ (as in Definition 1) with respect to network \mathcal{N} and input \mathbf{x} .*

Proof. The for-loop from Line 6 indicates that Algorithm 1 goes through every each feature \mathbf{x}^i in input \mathbf{x} by traversing the set of indices $\Theta(\mathbf{x})$. Line 5 means that π is one such instance of ordered traverse. When the iteration ends, all the indices in $\Theta(\mathbf{x})$ are either put into the irrelevant set of indices by $\mathbf{B} \mapsto \mathbf{B}'$ as in Line 11 or the explanation index set by $\mathbf{A} \mapsto \mathbf{A} \cup \{i\}$ as in Line 12. That is, \mathbf{A} and \mathbf{B} are two disjoint index sets forming $\Theta(\mathbf{x})$; in other words, $\mathbf{B} = \Theta(\mathbf{x}) \setminus \mathbf{A}$. Therefore, combined with Lemma 1, when the reasoner CHECK is sound, once iteration finishes we have the following specification

$$(\|\hat{\chi}^{\mathbf{B}} - \chi^{\mathbf{B}}\|_p \leq \epsilon) \wedge (\hat{\chi}^{\Theta \setminus \mathbf{B}} = \chi^{\Theta \setminus \mathbf{B}}) \Rightarrow |\hat{c} - c| \leq \delta.$$

holds on network \mathcal{N} , where $\hat{\chi}^{\mathbf{B}}$ is the variable representing all the possible assignments of irrelevant features $\mathbf{x}^{\mathbf{B}}$, i.e.,

$\forall \mathbf{x}^{\mathbf{B}'}$, and the pre-condition $\hat{\chi}^{\Theta \setminus \mathbf{B}} = \chi^{\Theta \setminus \mathbf{B}}$ fixes the values of the explanation features of an instantiated input \mathbf{x} . Meanwhile, the post-condition $|\hat{c} - c| \leq \delta$ where $c \mapsto \mathcal{N}(\mathbf{x})$ as in Line 4 ensures prediction invariance such that δ is 0 for classification and otherwise a pre-defined allowable amount of perturbation for regression. To this end, for some specific input \mathbf{x} we have the following property

$$\forall \mathbf{x}^{\mathbf{B}'}, (\|\mathbf{x}^{\mathbf{B}'} - \mathbf{x}^{\mathbf{B}}\|_p \leq \epsilon) \Rightarrow |\mathcal{N}(\mathbf{x}') - \mathcal{N}(\mathbf{x})| \leq \delta.$$

holds. Here we prove by construction. According to Definition 1, if the irrelevant features $\mathbf{x}^{\mathbf{B}}$ satisfy the above property, then we call the rest features $\mathbf{x}^{\mathbf{A}}$ a *guaranteed explanation* with respect to network \mathcal{N} and input \mathbf{x} . \square

A.3 Proof for Theorem 2

Theorem 2 (Optimality). *If CHECK is sound and complete, the guaranteed explanation $\mathbf{x}^{\mathbf{A}}$ returned by Algorithm 1 is optimal (as in Definition 2).*

Proof. We prove this by contradiction. From Definition 2 of optimal explanation, we know that explanation $\mathbf{x}^{\mathbf{A}}$ is optimal if, for any feature χ in explanation, there always exists an ϵ -perturbation on χ and the irrelevant features $\mathbf{x}^{\mathbf{B}}$ such that the prediction alters. Let us suppose $\mathbf{x}^{\mathbf{A}}$ is not optimal, then there exists a feature χ in $\mathbf{x}^{\mathbf{A}}$ such that no matter how to manipulate this feature χ' and the irrelevant features $\mathbf{x}^{\mathbf{B}'}$, the prediction always remains the same. That is,

$$\begin{aligned} \forall \mathbf{x}^{\mathbf{B}'}, \chi', & (\|(\mathbf{x}^{\mathbf{B}} \oplus \chi) - (\mathbf{x}^{\mathbf{B}'} \oplus \chi')\|_p \leq \epsilon) \\ & \Rightarrow |\mathcal{N}(\mathbf{x}) - \mathcal{N}(\mathbf{x}')| \leq \delta, \end{aligned}$$

where \oplus denotes concatenation of two features. When we pass this input \mathbf{x} and network \mathcal{N} into the VERIX framework, suppose Algorithm 1 examines feature χ at the i th iteration, then as in Line 7, the current irrelevant set of indices is $\mathbf{B}' \mapsto \mathbf{B} \cup \{i\}$, and accordingly the pre-conditions are $\phi \mapsto$

$$(\|\hat{\chi}^{\mathbf{B} \cup \{i\}} - \chi^{\mathbf{B} \cup \{i\}}\|_p \leq \epsilon) \wedge (\hat{\chi}^{\Theta \setminus (\mathbf{B} \cup \{i\})} = \chi^{\Theta \setminus (\mathbf{B} \cup \{i\})}).$$

Because $\hat{\chi}^{\mathbf{B} \cup \{i\}}$ is the variable representing all the possible assignments of irrelevant features $\mathbf{x}^{\mathbf{B}}$ and the i th feature χ , i.e., $\forall \mathbf{x}^{\mathbf{B}'}, \chi'$, and meanwhile

$$\hat{\chi}^{\Theta \setminus (\mathbf{B} \cup \{i\})} = \chi^{\Theta \setminus (\mathbf{B} \cup \{i\})}$$

indicates that the other features are fixed with specific values of this \mathbf{x} . Thus, with $c \mapsto \mathcal{N}(\mathbf{x})$ in Line 4, we have the specification $\phi \Rightarrow |\hat{c} - c| \leq \delta$ holds on input \mathbf{x} and network \mathcal{N} . Therefore, if the reasoner CHECK is sound and complete,

$$\text{CHECK}(\mathcal{N}, \phi \Rightarrow |\hat{c} - c| \leq \delta)$$

will always return True. Line 10 assigns True to HOLD, and index i is then put into the irrelevant set \mathbf{B} thus feature χ in the irrelevant features $\mathbf{x}^{\mathbf{B}}$. However, based on the assumption, feature χ is in explanation $\mathbf{x}^{\mathbf{A}}$, so χ is in $\mathbf{x}^{\mathbf{A}}$ and $\mathbf{x}^{\mathbf{B}}$ simultaneously – a contradiction occurs. Therefore, Theorem 2 holds. \square

B Model Specifications

Apart from those experimental settings in Section 4, we include detailed model specifications for reproducibility and reference purposes. Although evaluated on the Modified National Institute of Standards and Technology (MNIST) (Le-Cun, Cortes, and Burges 2010), German Traffic Sign Recognition Benchmark (GTSRB) (Stallkamp et al. 2012), and TaxiNet (Julian, Lee, and Kochenderfer 2020) image datasets – MNIST and GTSRB in classification and TaxiNet in regression, our VERIX framework can be generalised to other machine learning applications such as natural language processing.

As for the sub-procedure `CHECK` of Algorithm 1, while VERIX can potentially incorporate existing automated reasoners, we deploy the neural network verification tool Marabou (Katz et al. 2019). While it supports various model formats such as .pb from TensorFlow and .h5 from Keras, we employ the cross platform .onnx format for better Python API support. When importing a model with softmax as the final activation function, we remark that, for the problem to be *decidable*, one needs to specify the `outputName` parameter of the `read_onnx` function as the pre-softmax logits. As a workaround for this, one can also train the model without softmax in the last layer and instead use the `SoftmaxLoss` loss function from the `tensorflow_ranking` package. Either way, VERIX produces consistent results.

B.1 MNIST

For MNIST, we train a fully-connected feed-forward neural network with 3 dense layers activated with ReLU (first 2 layers) and softmax (last classification layer) functions as in Table 5, achieving 92.26% accuracy. While the MNIST dataset can easily be trained with accuracy as high as 99.99%, we are more interested in whether a very simple model as such can extract sensible explanations – the answer is yes. Meanwhile, we also train several more complicated MNIST models, and observe that their optimal explanations share a common phenomenon such that they are relatively more scattered around the background compared to the other datasets. This cross-model observation indicates that MNIST models need to check both the presence and absence of white pixels to recognise the handwritten digits correctly. Besides, to show the scalability of VERIX, we also deploy incomplete verification on state-of-the-art model structure as in Table 6.

B.2 GTSRB

As for the GTSRB dataset, since it is not as identically distributed as MNIST, to avoid potential distribution shift, instead of training a model out of the original 43 categories, we focus on the top first 10 categories with highest occurrence in the training set. This allows us to obtain an appropriate model with high accuracy – the convolutional model we train as in Table 7 achieves a test accuracy of 93.83%. It is worth mentioning that, our convolutional model is much more complicated than the simple dense model in (Ignatiev, Narodytska, and Marques-Silva 2019), which only contains one hidden layer of 15 or 20 neurons trained to distinguish two MNIST digits. Also, as shown in Table 4, we report results on the state-of-the-art GTSRB classifier in Table 8.

B.3 TaxiNet

Apart from the classification tasks performed on those standard image recognition benchmarks, our VERIX approach can also tackle regression models, applicable to real-world safety-critical domains. In this vision-based autonomous aircraft taxiing scenario (Julian, Lee, and Kochenderfer 2020) of Figure 9, we train the regression mode in Table 9 to produce an estimate of the cross-track distance (in meters) from the ownship to the taxiway centerline. The TaxiNet model has a mean absolute error of 0.824 on the test set, with no activation function in the last output layer.

B.4 Dense, Dense (large), and CNN

In Section 4.6, we analyse execution time of VERIX on three models with increasing complexity: Dense, Dense (large), and CNN as in Tables 10, 11, and 12, respectively. To enable a fair and sensible comparison, those three models are used across the MNIST, TaxiNet, and GTSRB datasets with only necessary adjustments to accommodate each task. For example, in all three models $h \times w \times c$ denotes different input size height \times width \times channel for each dataset. For the activation function of the last layer, softmax is used for MNIST and GTSRB while TaxiNet as a regression task needs no such activation. Finally, TaxiNet deploys `he_uniform` as the `kernel_initializer` parameter in the intermediate dense and convolutional layers for task specific reason.

Layer Type	Parameter	Activation
Input	$28 \times 28 \times 1$	–
Flatten	–	–
Fully Connected	10	ReLU
Fully Connected	10	ReLU
Fully Connected	10	softmax

Table 5: Architecture for the MNIST classifier.

Type	Parameter	Activation
Input	$28 \times 28 \times 1$	–
Convolution	$3 \times 3 \times 32$	ReLU
Convolution	$3 \times 3 \times 32$	ReLU
MaxPooling	2×2	–
Convolution	$3 \times 3 \times 64$	ReLU
Convolution	$3 \times 3 \times 64$	ReLU
MaxPooling	2×2	–
Flatten	–	–
Fully Connected	200	ReLU
Dropout	0.5	–
Fully Connected	200	ReLU
Fully Connected	10	softmax

Table 6: Architecture for the MNIST-sota classifier.

Type	Parameter	Activation
Input	$32 \times 32 \times 3$	–
Convolution	$3 \times 3 \times 4 (1)$	–
Convolution	$2 \times 2 \times 4 (2)$	–
Fully Connected	20	ReLU
Fully Connected	10	softmax

Table 7: Architecture for the GTSRB classifier.

Type	Parameter	Activation
Input	$28 \times 28 \times 1$	–
Convolution	$3 \times 3 \times 32$	ReLU
Convolution	$3 \times 3 \times 32$	ReLU
Convolution	$3 \times 3 \times 64$	ReLU
MaxPooling	2×2	–
Convolution	$3 \times 3 \times 64$	ReLU
Convolution	$3 \times 3 \times 64$	ReLU
MaxPooling	2×2	–
Flatten	–	–
Fully Connected	200	ReLU
Dropout	0.5	–
Fully Connected	200	ReLU
Fully Connected	10	softmax

Table 8: Architecture for the GTSRB-sota classifier.

Type	Parameter	Activation
Input	$27 \times 54 \times 1$	–
Flatten	–	–
Fully Connected	20	ReLU
Fully Connected	10	ReLU
Fully Connected	1	–

Table 9: Architecture for the TaxiNet regression model.

Layer Type	Parameter	Activation
Input	$h \times w \times c$	–
Flatten	–	–
Fully Connected	10	ReLU
Fully Connected	10	ReLU
Fully Connected	10 / 1	softmax / –

Table 10: Architecture for the Dense model.

Layer Type	Parameter	Activation
Input	$h \times w \times c$	–
Flatten	–	–
Fully Connected	30	ReLU
Fully Connected	30	ReLU
Fully Connected	10 / 1	softmax / –

Table 11: Architecture for the Dense (large) model.

Layer Type	Parameter	Activation
Input	$h \times w \times c$	–
Convolution	$3 \times 3 \times 4$	–
Convolution	$3 \times 3 \times 4$	–
Fully Connected	20	ReLU
Fully Connected	10 / 1	softmax / –

Table 12: Architecture for the CNN model.